A novel method for load line displacement rate partitioning in creep crack growth tests on Type 316H Stainless Steel

M. D. Jones[1], D. W. Dean[2], D. Hughes[2], C. M. Davies[1]

[1]Department of Mechanical Engineering, Imperial College London, London, SW7 2AZ

[2]EDF Energy, Barnett Way, Barnwood, Gloucester, GL4 3RS

Abstract

Characterising the creep crack growth behaviour of Type 316H stainless steel is vital in obtaining accurate predictions for the lifetime of high temperature components, for example in UK advanced gas cooled reactors. The correlation between creep crack growth rates and the fracture mechanics parameter C^*, considered to govern the crack growth process, is obtained from creep crack growth tests. The C^* parameter is experimentally determined using an expression which requires knowledge of the load line displacement rate due to creep. Historically this has been calculated by subtracting values for the elastic and plastic contributions to the load line displacement, obtained from available solutions from the total experimentally measured load line displacement. However, the solutions available to determine the plastic contribution rely on generating a power-law fit to uniaxial tensile data, which is difficult to accomplish accurately over a large stress range. In addition, these expressions cannot account for strain history effects during crack growth. Consequently the elastic and plastic contributions are often erroneously large and can even be in excess of the experimental total load line displacement. A novel technique has been proposed to provide improved estimates of the creep contribution to the load line displacement rates during creep crack growth tests. This technique employs finite element analysis that incorporates material specific uniaxial tensile test data to simulate crack growth in an experimental test. A single elastic-plastic-creep simulation is used to determine the separate elastic-plastic and creep contributions to the load line displacement, meaning that, unlike historic analyses, creep stress relaxation and strain history effects can now be accounted for. The results have demonstrated that advanced predictions of the creep contributions to the load line displacement can be obtained using this technique.

Keywords

Creep crack growth, 316H stainless steel, C*

Nomenclature

a	Crack length
$\dot{a}$	Crack growth rate
$\dot{a}_s$	Steady state creep crack growth rate
c	Ligament length
h_3	Fully plastic solution corresponding to the load line displacement
n	Temperature dependent secondary creep material constant
n_p	Temperature dependent primary creep material constant
p	Temperature dependent primary creep material constant
t	Time
A	Temperature dependent secondary creep material constant
A_p	Temperature dependent primary creep material constant
B	Specimen thickness
B_{eff}	Effective specimen thickness
B_{net}	Net specimen thickness
C^*	Steady state creep fracture mechanics parameter
D	Steady state creep crack growth material constant
E'	Effective elastic modulus
H	Geometry dependent numerical factor
J_p	Plastic contribution to the J-integral
K	Stress intensity factor
N	Hardening exponent for a power-law fit
P	Applied load
P_0	Limit load per unit thickness
V_2	Geometric function in elastic compliance function
W	Specimen width
α	Material constant for a power law-fit
ε_p	Primary creep strain
$\dot{\varepsilon}_p$	Primary creep strain rate
ε_{p0}	Yield strain
$\dot{\varepsilon}_s$	Secondary creep strain
η	Geometry dependent numerical factor
σ	Stress
σ_{p0}	Yield stress
ϕ	Steady state creep crack growth index
Δ_c	Creep contribution to the load line displacement
$\dot{\Delta}_c$	Creep contribution to the load line displacement rate
Δ_e	Elastic contribution to the load line displacement
$\dot{\Delta}_e$	Elastic contribution to the load line displacement rate
Δ_{ep}	Elastic-plastic contribution to the load line displacement
Δ_p	Plastic contribution to the load line displacement
$\dot{\Delta}_p$	Plastic contribution to the load line displacement rate
Δ_T	Total load line displacement
$\dot{\Delta}_T$	Total load line displacement rate

CCG	Creep Crack Growth
C(T)	Compact Tension
FEA	Finite Element Analysis
LLD	Load Line Displacement
PD	Potential Drop

1. Introduction

Creep Crack Growth (CCG) analyses are important for assessing the structural integrity of high temperature power plant to predict the remaining lifetime of components. The steady state CCG rate is expected to be described by a power-law correlation with the fracture mechanics parameter $\boldsymbol{C}^*$ [1]. Calculating experimental values for $\boldsymbol{C}^*$ requires determination of the Load Line Displacement (LLD) rate due to creep, $\dot{\Delta}_c$. This cannot be measured directly, and must instead be found by partitioning the total displacement rate, $\dot{\Delta}_T$ into the three contributions due to elasticity, $\dot{\Delta}_e$, plasticity, $\dot{\Delta}_p$, and creep. Historically this has been achieved by determining $\dot{\Delta}_e$ and $\dot{\Delta}_p$ using theoretical expressions and subtracting them from $\dot{\Delta}_T$ [2], *i.e.*,

$$\dot{\Delta}_c = \dot{\Delta}_T - \dot{\Delta}_e - \dot{\Delta}_p \tag{1}$$

To determine $\dot{\Delta}_p$, the testing standards assume that the material's tensile response can be described by the Ramberg-Osgood material model, *i.e.* deformation plasticity formulation, however, this can result in negative values for $\dot{\Delta}_c$ [3][4]. As illustrated in Figure 1, for 316H stainless steel at 550°C, the Ramberg-Osgood model's best fit to the data does not accurately represent the stress-strain behaviour over a large stress range [5], this can lead to an overestimation of the plastic contribution to the load line displacement and thus erroneous, negative values of $\dot{\Delta}_c$.

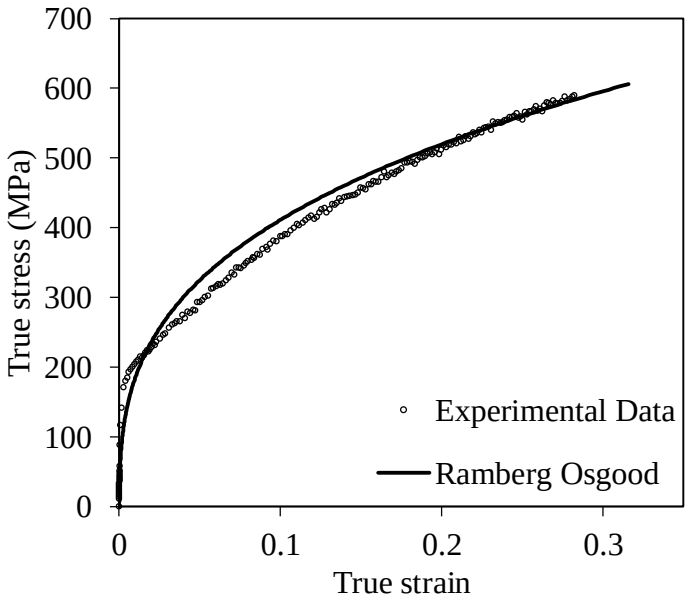


Figure 1 – Comparison of experimental uniaxial tensile data with Ramberg-Osgood fit for Type 316H

To overcome the issue of obtaining negative values of $\dot{\Delta}_c$, $\dot{\Delta}_T$ is often employed in the expression to calculate $\boldsymbol{C}^*$ instead of $\dot{\Delta}_c$. This is based on the assumption that if the crack growth is predominantly a result of creep deformation then $\dot{\Delta}_e$ and $\dot{\Delta}_p$ may be only a small proportion of $\dot{\Delta}_T$. However, for accelerated CCG tests on Type 316H steel high loads must be imposed on specimens

in order to complete tests within a practical timeframe. Type 316H has a very low yield stress at high temperatures, and therefore experiences a large amount of plastic deformation under the high loads which cannot be neglected when determining $\dot{\Delta}_c$.

It is proposed in this work that accurate values for $\dot{\Delta}_e$ and $\dot{\Delta}_p$ may be determined by using actual tensile test data, i.e. an 'incremental plasticity' formulation, implemented through Finite Element Analysis (FEA) rather than assuming a Ramberg-Osgood power-law fit. Separate elastic, elastic-plastic and elastic-plastic-creep simulations have been run, from which the individual displacements and displacement rates could be determined. Comparisons have been made between the FEA results and the LLD values calculated using the theoretical expressions. The FEA should yield more accurate experimental estimates of $\boldsymbol{C}^*$ and may lead to improved correlation with the CCG rate during the early stages of a test.

2. Theoretical Relations

2.1. Creep

Creep is commonly modelled using power-law relationships. Primary creep may be appreciable for 316H under the relevant test conditions, and it may be modelled as [6]

$$\dot{\varepsilon}_p = pA_p{}^{1/p}\varepsilon_p{}^{1-1/p}\sigma^{n_p/p} \tag{2}$$

where $\dot{\varepsilon}_p$ is the primary creep strain rate, ε_p is the primary creep strain, p, A_p and n_p are temperature dependent primary creep material constants and σ is the stress.

Secondary creep deformation can be expressed by the Norton power-law relationship [7]

$$\dot{\varepsilon}_s = A\sigma^n \tag{3}$$

where $\dot{\varepsilon}_s$ is the secondary creep strain rate and A and n are the temperature dependent secondary creep material constants.

2.2. Creep Crack Growth

Creep crack growth rate is commonly characterised by the steady state creep fracture mechanics parameter $\boldsymbol{C}^*$ in the following relationship [1]

$$\dot{a}_s = DC^{*\phi} \tag{4}$$

where $\dot{a}_s$ is steady state CCG rate, D is a material constant and ϕ is an index slightly less than unity. This relationship requires $\boldsymbol{C}^*$ to be calculated throughout the test. Experimentally it cannot be calculated directly from the line integral definition, and so is determined using the expression [4]

$$C^* = \frac{P\dot{\Delta}_c}{B(W-a)} H\eta \tag{5}$$

where P is the applied load, B is the specimen thickness, W is the specimen width, a is the crack length and H and η are geometry dependent numerical factors. $\dot{\Delta}_c$ must be determined accurately in order to calculate reliable estimates for C^*. This requires the partitioning of the total response of the specimen, and therefore determination of the separate elastic and plastic response which may be subtracted from the total response to give the creep contribution, as shown in Equation (1).

2.3. Elastic-Plastic Response

The plastic deformation behaviour of the material has previously been assumed to adhere to a power-law fit to uniaxial tensile data. This would take the form of a Ramberg-Osgood law, the normalised version of which is

$$\frac{\varepsilon}{\varepsilon_{p0}} = \frac{\sigma}{\sigma_{p0}} + \alpha\left(\frac{\sigma}{\sigma_{p0}}\right)^N \tag{6}$$

where ε is the strain, σ_{p0} is the normalising stress (often taken as the 0.2% proof stress), ε_{p0} is the normalising strain (often taken to be σ_{p0}/E), σ is the stress, α is a material constant for the power-law fit and N is the hardening exponent for the power-law fit. The values for the power-law fit parameters are given below in Table 1

Table 1 – Ramberg-Osgood material model parameter values

Parameter	Value
α	6.42
N	3
σ_{p0} (MPa)	170
ε_{p0}	1.073×10^{-3}

The historical method for determining the elastic-plastic contribution to the LLD has been to calculate the LLD rate directly using the expressions given in ASTM E1457, which are based on the EPRI solutions [8]. The tests considered in this paper used Compact Tension, C(T), specimens, and all of the following expressions are appropriate for this test geometry.

The EPRI solution for the elastic contribution to the LLD is [8]

$$\Delta_e = \frac{1}{E'} V_2(a/W) P \tag{7}$$

where $V_2(a/W)$ is defined as

$$V_2(a/W) = \left(\frac{1 + a/W}{1 - a/W}\right)^2 [2.163 + 12.219(a/W) - 20.065(a/W)^2 - 0.9925(a/W)^3 + 20.609(a/W)^4 - 9.9314(a/W)^5] \quad (8)$$

The EPRI solution for the plastic contribution to the LLD is [8]

$$\Delta_p = \alpha \varepsilon_{p0} a h_3(a/W, N)(P/P_0)^N \quad (9)$$

where h_3 is the fully plastic solution corresponding to the LLD and P_0 is the limit load per unit thickness. This is calculated as

$$P_0 = 1.455 \eta c \sigma_{p0} \quad (10)$$

for plane strain and

$$P_0 = 1.071 \eta c \sigma_{p0} \quad (11)$$

for plane stress. For both the above, c is the ligament length $(W - a)$, and η is defined as [8]

$$\eta = [(2\,a/c)^2 + 2(2\,a/c) + 2]^{0.5} - 2[a/c + 1] \quad (12)$$

The ASTM standard gives the time derivatives of the elastic and plastic contribution to the LLD, these rates are expressed as [2]

$$\dot{\Delta}_e = \frac{2BK^2\dot{a}}{PE'} \quad (13)$$

$$\dot{\Delta}_p = \frac{\dot{a}BJ_p(N+1)}{P} \quad (14)$$

where K is the stress intensity factor, $\dot{a}$ is the crack growth rate, E' is the effective elastic modulus and J_p is the plastic contribution to the J parameter. In this work, values for the LLD components have been determined using the EPRI solutions, and these values were differentiated with respect to time to determine the respective rates. This gives identical rates to that determined using the ASTM LLD rate expressions.

There are issues associated with this approach. Fitting the Ramberg-Osgood model is subject to variability and can lead to significant error [5]. A range of fitting parameters can lead to a similar fit. Additionally, it is difficult to fit the model over a large range of stress and strain, and therefore it must be decided whether it is beneficial to only fit the model accurately over a small range of interest or to try and attain a reasonable global fit, although a wide range of stresses can exist in the vicinity of the crack tip so a global fit is likely to be more appropriate.

3. Finite Element Analysis

It is proposed that a more accurate determination of the elastic-plastic contribution to the LLD, Δ_{ep}, would be obtained using material tensile data in FEA, employing an incremental plasticity formulation. To prove this, FEA has been performed simulating a relatively high load (short term) and low load (long term) CCG test. A description of the analysis undertaken is given in the following sub sections.

3.1. Creep Crack Growth Test Simulation

Two CCG tests on Compact Tension, C(T), samples were simulated using the FEA software package Abaqus, one relatively short term [9], loaded to the plane strain plastic limit load, P_0, and one relatively long term [3], loaded to $0.7P_0$. This allowed for comparison of specimens with different levels of initial plastic deformation and creep rates throughout the test. One of the main uses for Type 316H is in the boilers of nuclear Advanced Gas Cooled Reactors which typically operate at temperatures around 500-550°C. Tests are often carried out at the highest temperature of 550°C to ensure conservative results and to minimise test durations. Both of these tests were carried out at this temperature. The test details are given below in Table 2. The effective thickness is determined by

$$B_{eff} = \sqrt{\frac{B_{net}}{B}} B \tag{15}$$

where B_{net} is the net thickness of the specimen between the side grooves.

Table 2 – Test details

Test	Short term	Long term
Width, W (mm)	50.00	37.91
Effective Thickness, B_{eff} (mm)	22.36	16.97
Initial Crack Length, a_0 (mm)	25.00	20.68
a_0/W	0.50	0.55
Initial Stress Intensity Factor (MPa√m)	47.3	26.6
P/P_0 Plane strain	1.0	0.7
Test Duration (hours)	742	16630
Crack Initiation Time (hours)	297	1384

The crack growth data were obtained using the Potential Drop (PD) technique [10]. The PD data for both tests has been analysed according to the assumption that initiation occurs at the point of inflection on a plot of PD against LLD of the specimen [11]. **Error! Reference source not found.**This method more accurately captures incubation periods and the creep crack initiation point. It gives an improved interpretation of the data over the previous technique which assumed that crack initiation occurred after an increase in the PD value corresponding to a set amount of crack growth, normally 0.2 mm [12]. The crack growth profiles for both tests are shown in Figure 2 and Figure 3.

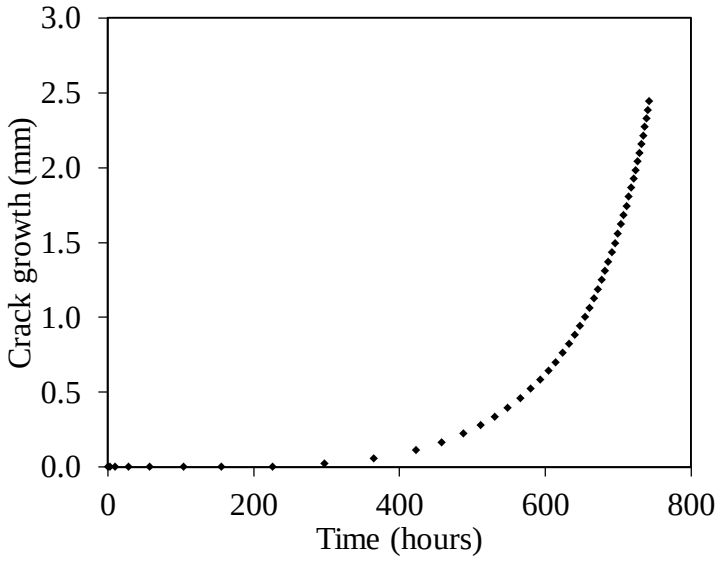


Figure 2 – Short term crack growth profile [9]

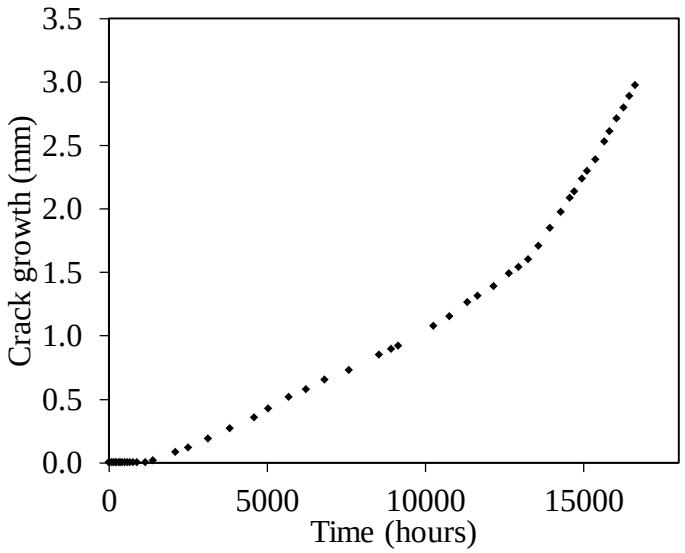


Figure 3 – Long term crack growth profile [3]

3.2. Load Line Displacement Partitioning Procedure

Three separate finite element models were run for each experimental test. These simulated elastic, elastic-plastic and elastic-plastic-creep deformation behaviour. The LLD values with respect to time were extracted from the results of each simulation. The LLD rate was determined by means of a 7 point incremental polynomial method [2]. Each individual contribution was calculated from these simulations according to Table 3.

Table 3 – Load line displacement rate contributions

Material behaviour	Contribution
Elastic	$\dot{\Delta}_e$
Elastic-plastic	$\dot{\Delta}_{ep} = \dot{\Delta}_e + \dot{\Delta}_p$
Elastic-plastic-creep	$\dot{\Delta}_{epc} = \dot{\Delta}_e + \dot{\Delta}_p + \dot{\Delta}_c$
Plastic	$\dot{\Delta}_p = \dot{\Delta}_{ep} - \dot{\Delta}_e$
Creep	$\dot{\Delta}_c = \dot{\Delta}_{epc} - \dot{\Delta}_{ep}$

3.3. Material Model

The plastic deformation behaviour was modelled using uniaxial test data for Type 316H at 550°C, as shown in Figure 1. The creep deformation behaviour was modelled using a user defined creep subroutine. This subroutine calculates the primary and secondary creep strain increments using the following expressions which may be determined from Equations (2) and (3). The primary creep strain increment using a strain hardening model is equal to

$$\Delta\varepsilon_p = \left[\varepsilon^{1/p} + (A_p\sigma^{n_p})^{1/p}\Delta t\right]^p - \varepsilon \tag{16}$$

where t is time, and the secondary strain increment is equal to

$$\Delta\varepsilon_s = A\sigma^n\Delta t \tag{17}$$

Having determined both the primary and secondary creep strain increment at a point in time, the two values are compared and the larger of the two is used. This is because if the secondary creep strain increment is larger than the primary creep strain increment the behaviour must have switched to secondary creep. The primary and secondary creep parameters are given in Table 4.

Table 4 – Creep parameters for Type 316H at 550°C [13]

Parameter	Value
A_p ($\mathrm{MPa^{-n_p}h^{-p}}$)	2.60×10^{-23}
p	0.746
n_p	7.45
A ($\mathrm{MPa^{-n}h^{-1}}$)	1.559×10^{-35}
n	11.95

3.4. Mesh

3.4.1. 2D Mesh

For the 2D mesh, half of a C(T) sample was modelled as shown in Figure 4, employing y-symmetry conditions along the uncracked ligament. The mesh was refined in the crack growth region as shown in Figure 5, and is coarse over the majority of the specimen to improve computational efficiency. The mesh was developed for a standard C(T) specimen of width 50 mm, with crack growth elements of dimensions 0.02 mm square. The mesh was scaled by a factor of ~0.76 to give the dimensions of the smaller specimen for the long term test. The crack growth elements were then 0.0152 mm square. The mesh consists of 19716 elements and 20027 nodes. CPE4H elements and CPS4R elements were used for the plane strain and plane stress simulations, respectively. The appropriate load was applied in the y-direction at the load point.

The crack growth simulation comprised of alternating elastic-plastic (*Static) and creep (*Visco) steps. The initial static step involved loading the specimen, which was followed by a creep step that lasted the duration of the creep crack incubation period (period of time prior to creep crack extension). At the end of the creep step, the y-symmetry condition was removed from the appropriate node to simulate crack extension and the simulation moves onto the next static step then creep step etc. This sequence of y-symmetry condition release, static and creep steps was repeated as the crack advanced incrementally.

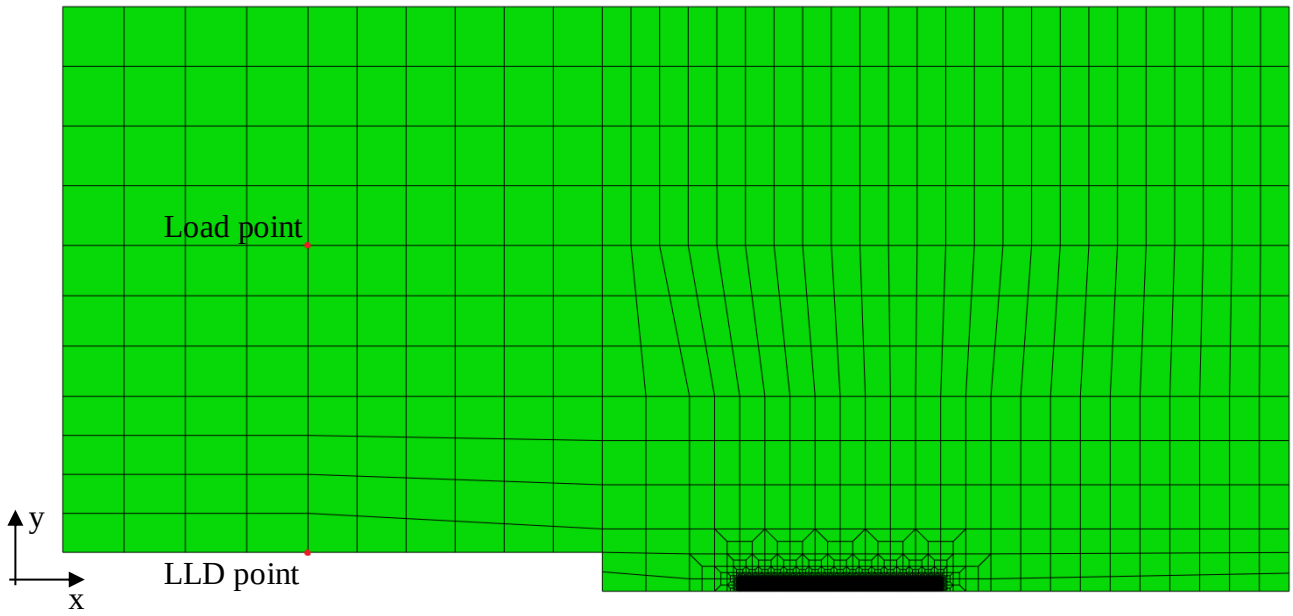


Figure 4 – 2D mesh

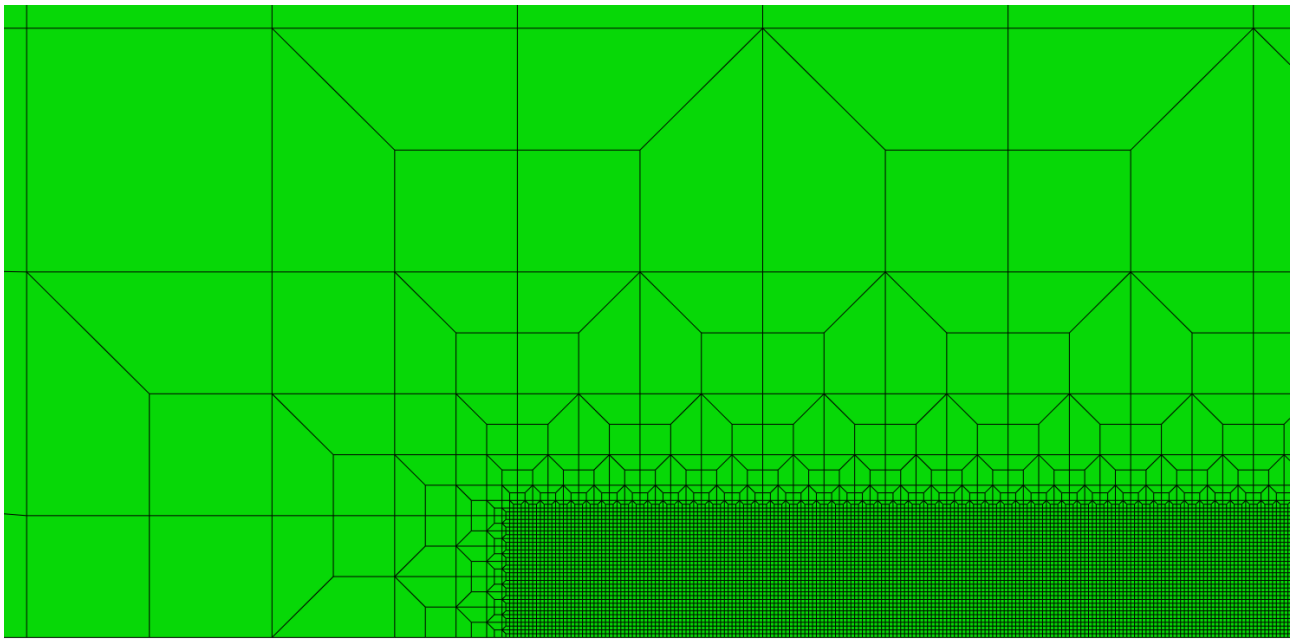


Figure 5 – Enlarged view of the crack tip region illustrating the mesh transition from coarse to fine

3.4.2. 3D Mesh

For the 3D mesh a quarter section of a side-grooved C(T) sample was modelled as shown in Figure 6, employing symmetry conditions to reduce computational time. The load was applied to a point coincident with both the axis of the pinhole and what would be the mid-plane of the full sample. This point was constrained by means of a kinematic coupling to all nodes on the inner surface of the pinhole. This method eliminates the issues that can occur when modelling a separate pin with a contact interaction on the pinhole. The mesh is composed of 33810 C3D8R elements and 38209 nodes. The mesh was relatively coarse over the majority of the model for computational efficiency, becoming much finer in the crack growth region. A focused view of the transition from the coarse mesh to the fine crack region is shown in Figure 7. As with the 2D model, the 3D model was developed for a standard C(T) specimen of width 50 mm where the crack growth elements are 0.1 mm square in the x-y plane, and the mesh was again scaled by a factor of ~0.76 to produce the mesh for the long term test which gave crack growth elements 0.076 mm long. The crack growth was implemented in the same manner as for the 2D model.

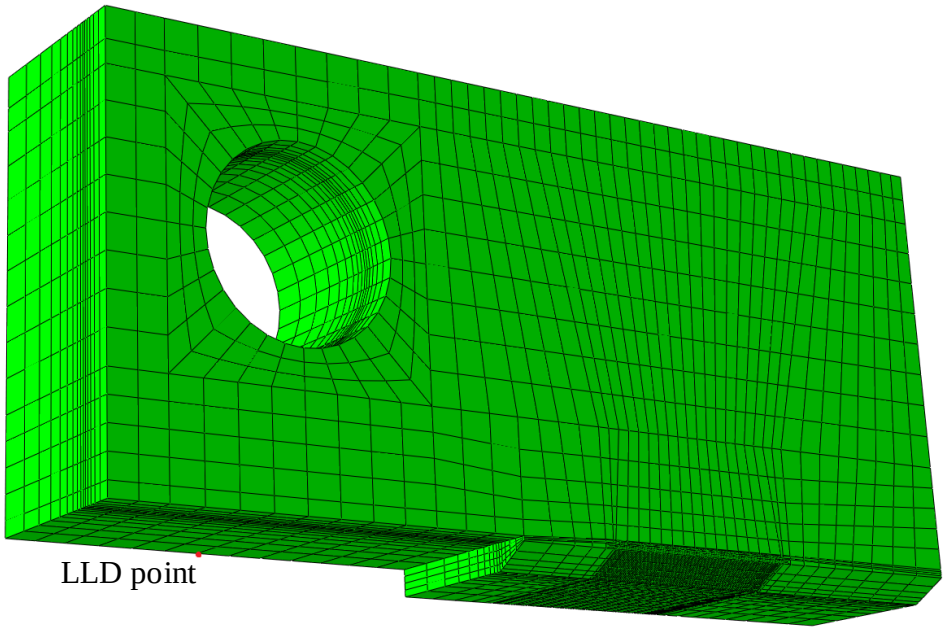


Figure 6 – 3D Mesh

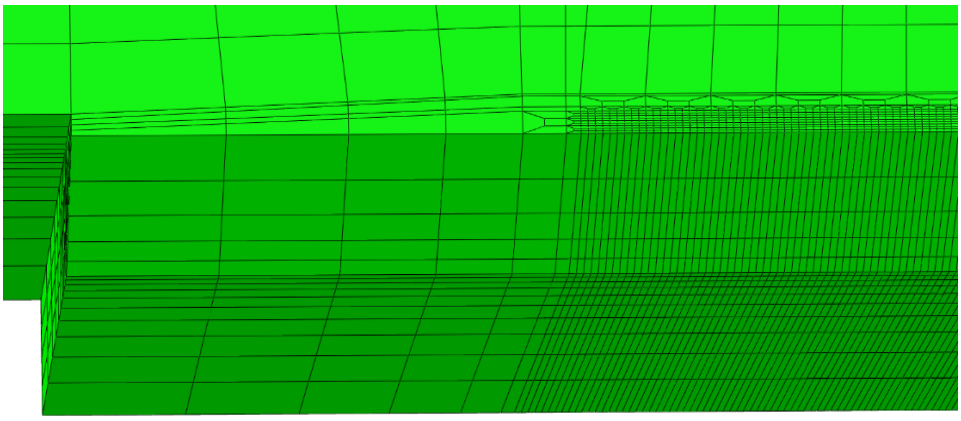


Figure 7 – Transition between coarse mesh and crack region

4. Results

In the following section the results from the FEA are compared with the EPRI solutions for the LLD and LLD rate. It should be noted that the LLD values from the FEA have been taken from the node on the bottom face of the specimen directly below the load point, as shown in Figure 4 and Figure 6, which represents the experimental LLD measurement positions using a capacitance gauge.

4.1. EPRI Solutions vs Finite Element Analysis

The results in this subsection compare the LLD as calculated by the EPRI solutions against those determined from the FEA. In order to make a direct comparison between the two methods, the results given are from the 2D FEA simulations. The LLD has been normalised with respect to the specimen width so that direct comparisons can be made between the two tests which featured specimens of different sizes. The comparisons are first made for the elastic contribution, Δ_e, and

then for the plastic contribution, Δ_p. It should be noted that the LLD shown here includes the load up portion to emphasise the contribution due to the instantaneous load.

4.1.1. Elastic Contribution

Firstly comparisons are made for the elastic contribution, Δ_e, determined from an elastic FEA model and the elastic compliance functions [8]. This provides validation of the FE meshes and the data required to determine Δ_p from the elastic-plastic analyses (see Table 3).

Figure 8 to Figure 11 below show normalised Δ_e and $\dot{\Delta}_e$ for plane strain (pε) and plane stress (pσ) in both the long and short term tests. Initially, during the incubation period of both tests, there is no further increase in Δ_e as the crack has not yet started to grow. Since the elastic response is independent of time, Δ_e will not change unless crack growth occurs. Post initiation, Δ_e increases as the crack grows due to the increased compliance of the sample. The plane strain results are lower than plane stress due to the effective Young's modulus being higher in plane strain. The higher stresses in the short term test caused higher values of normalised Δ_e, and the short term normalised $\dot{\Delta}_e$ was higher due to the faster crack growth. The results show strong agreement between FEA and EPRI for both stress states, as expected.

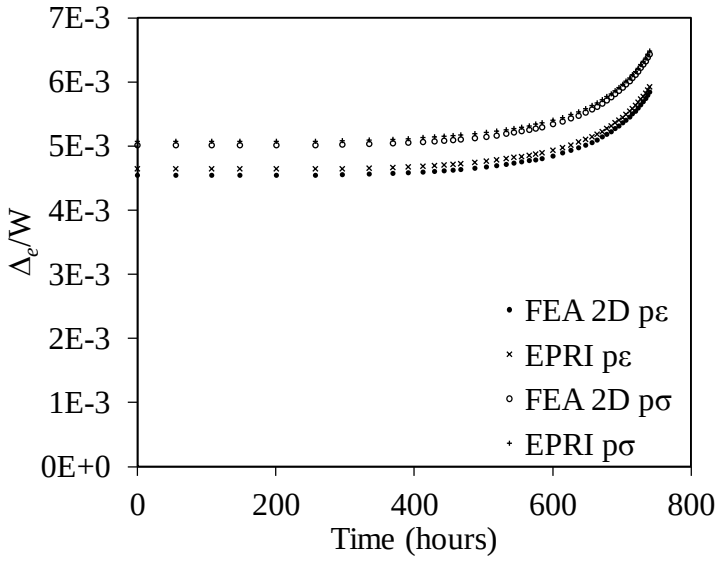


Figure 8 – Short term test normalised elastic contribution to the LLD

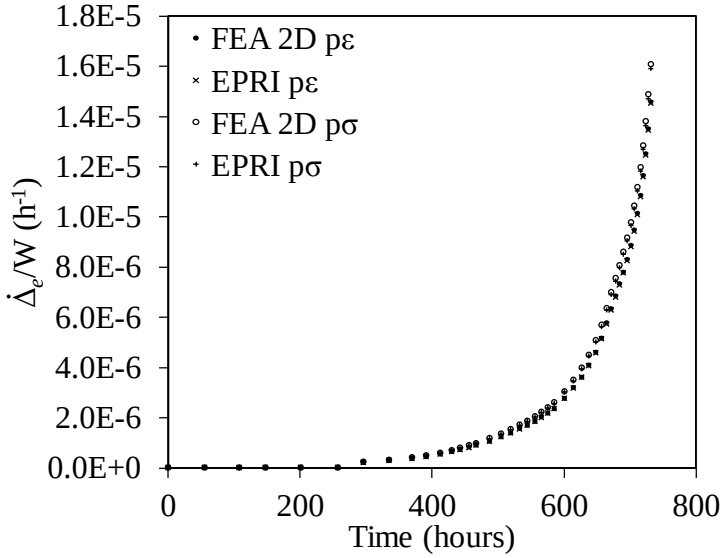


Figure 9 – Short term test normalised elastic contribution to the LLD rate

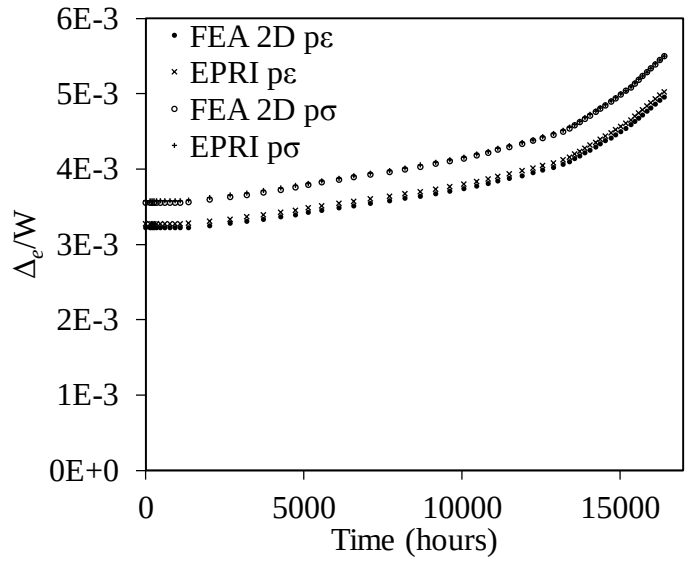


Figure 10 – Long term test normalised elastic contribution to the LLD

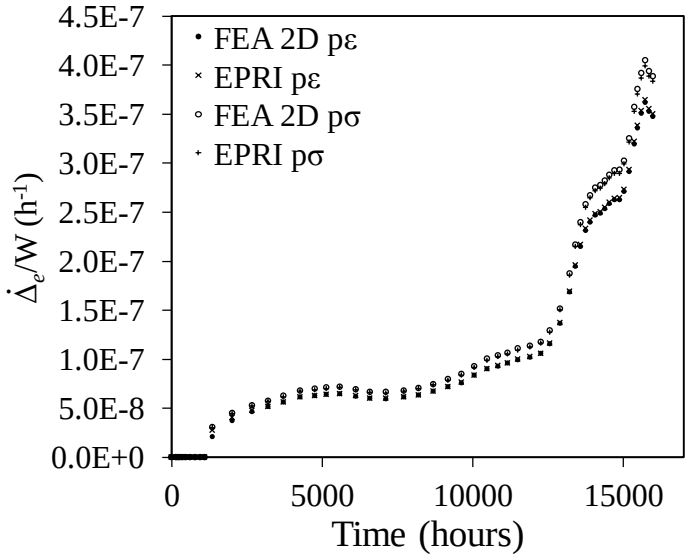


Figure 11 – Long term test normalised elastic contribution to the LLD rate

4.1.2. Plastic Contribution

The results in this subsection compare Δ_p as calculated by the EPRI solutions using the Ramberg-Osgood fit to the material's tensile data against those determined from the FEA using the actual material tensile data.

Figure 12 to Figure 15 below show the normalised Δ_p and $\dot{\Delta}_p$ values during the long and short term tests for both plane strain and plane stress conditions. As with the elastic contribution, Δ_p remains unchanged after the load has been applied until the crack initiates as it is also time independent. Δ_p then increases with crack growth as the stresses in the specimen increase, leading to further plastic deformation. The plane strain results are lower than plane stress due to the constraint effect which inhibits plastic deformation. The normalised $\dot{\Delta}_p$ is again higher in the short term test due to the faster CCG rate and the higher stresses in the short term test cause greater values of normalised Δ_p. As shown in Table 2 the short term test is at the limit load, whereas the long term test is only at 70% of the limit load and therefore Δ_p is a smaller contribution to the total LLD, Δ_T. In all cases the EPRI solution overestimates the FEA results. This confirms that solutions based on the Ramberg-Osgood fit to the tensile data are inaccurate and predict erroneously high values for Δ_p.

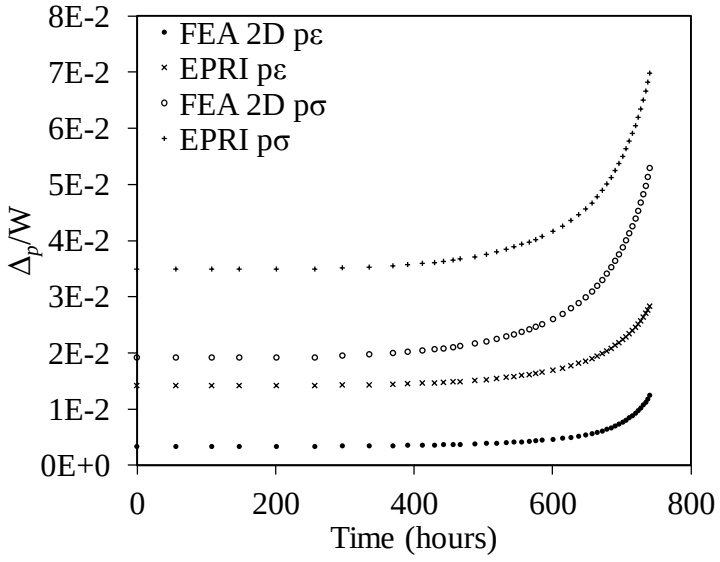


Figure 12 – Short term test normalised plastic contribution to the LLD

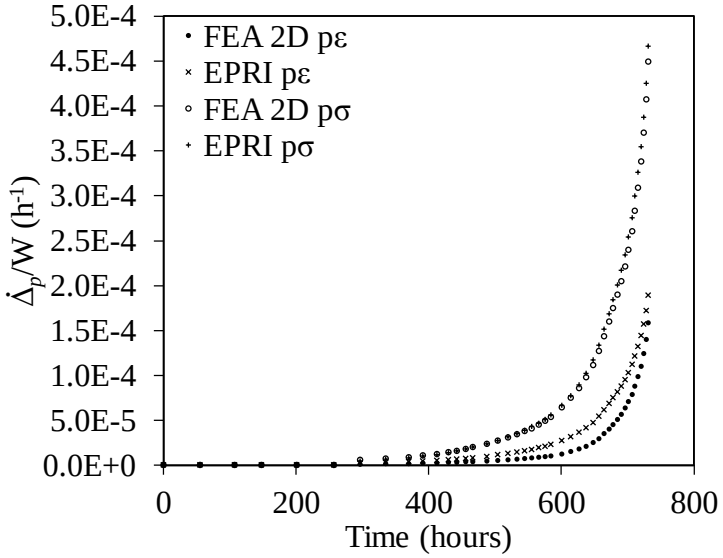


Figure 13 – Short term test normalised plastic contribution to the LLD rate

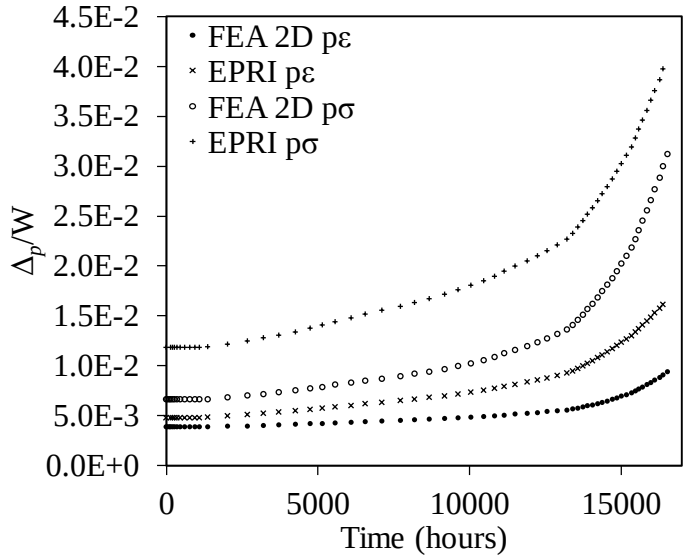


Figure 14 – Long term test normalised plastic contribution to the LLD

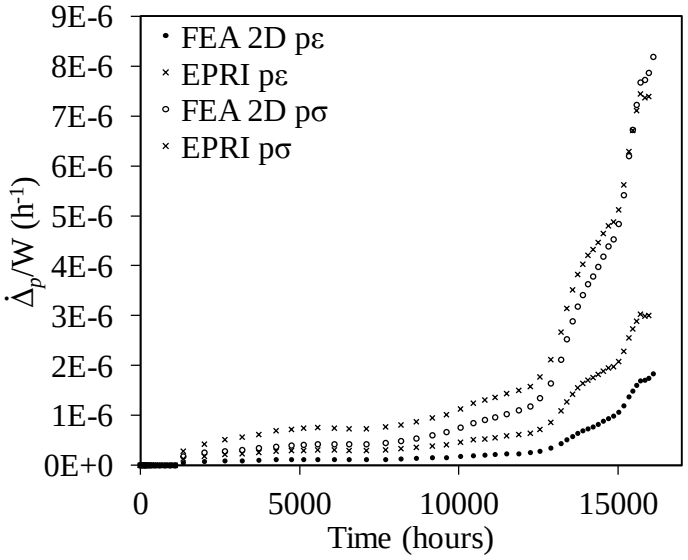


Figure 15 – Long term test normalised plastic contribution to the LLD rate

Comparisons can also be made between the Δ_p values calculated using the EPRI solutions and the experimental Δ_T (elastic-plastic-creep) values. This is shown for each test in Figure 16 and Figure 17. In this case, absolute values for the LLD are shown as a comparison is not made between the two tests. It can be seen that in both tests the EPRI solutions give results that significantly exceed the experimental Δ_T. This further proves that they do not yield accurate results.

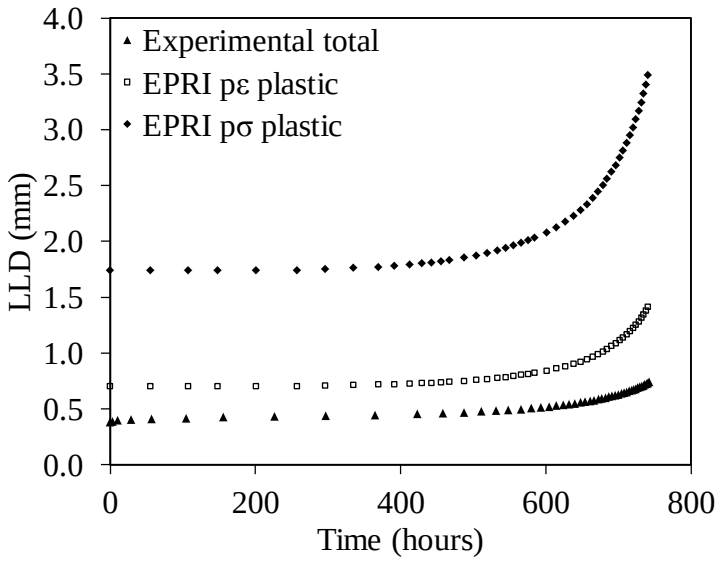


Figure 16 – Short term comparison of EPRI plastic LLD with total experimental LLD

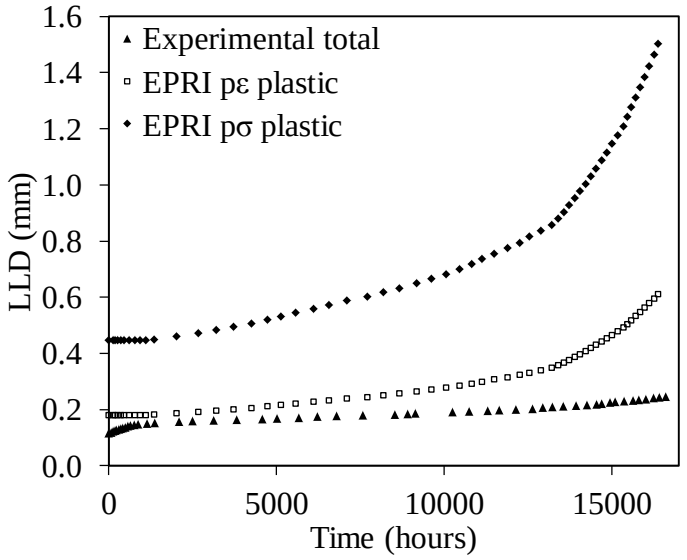


Figure 17 – Long term comparison of EPRI plastic LLD with total experimental LLD

4.2. 2D FEA vs 3D FEA

The results in this subsection compare the results for Δ_T from the 2D and 3D FEA models against each other to determine if either of the 2D stress states can be used as a good approximation for 3D. The comparisons are shown in Figure 18 and Figure 19. The 3D and 2D plane strain results show very strong agreement, indicating that the majority of the specimen is in plane strain and that a 2D plane strain model can be used in place of a 3D model with minimal error. It is beneficial to use 2D

as it is possible to have a much finer crack growth mesh for a similar level of computational capacity meaning that the behaviour around initiation can be more precisely characterised.

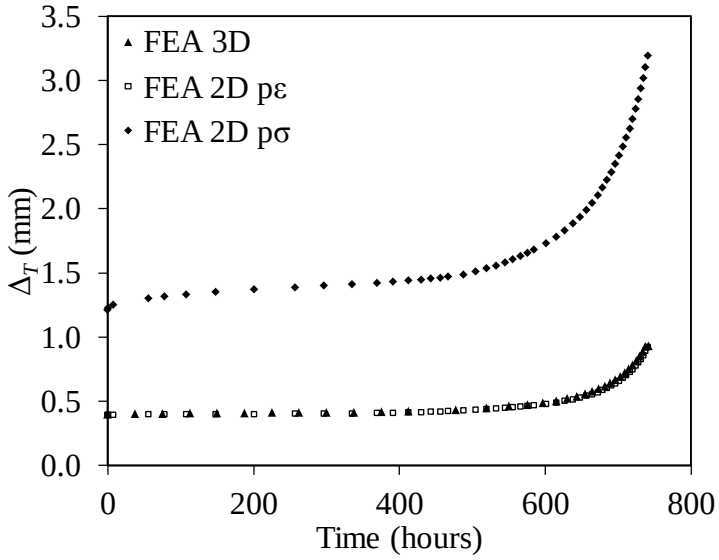


Figure 18 – Comparison of short term FEA 2D and FEA 3D total LLD

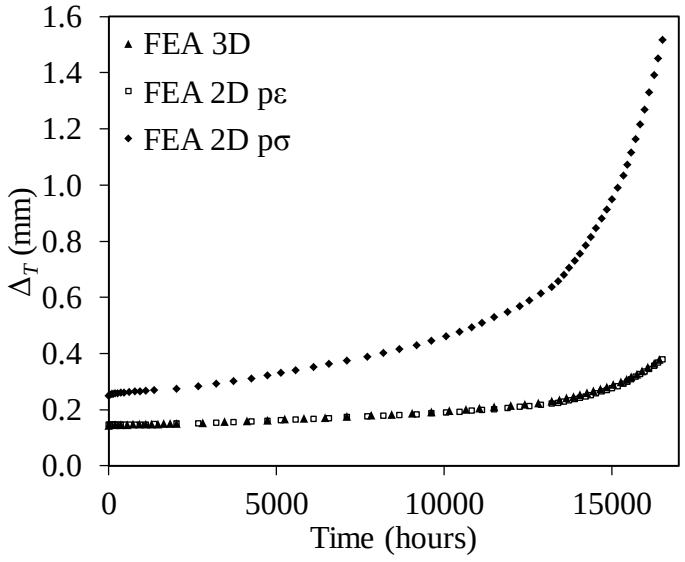


Figure 19 – Comparison of long term FEA 2D and FEA 3D total LLD

4.3. Creep Contribution

The results for Δ_c as determined by the current displacement partitioning process detailed in Section 3.2 are shown in the following sections. These contributions are determined first by subtracting Δ_{ep} from Δ_T in the FEA, and then by subtracting the FEA Δ_{ep} from the measured experimental Δ_T. All FEA results used are from 2D plane strain models. It should be noted that the 2D plane stress results for the elastic-plastic contribution exceeded the experimental data for the full duration of both tests, further confirming that it does not accurately represent the behaviour of the specimen and does not warrant any further consideration.

4.3.1. FEA Contribution

Figure 20 to Figure 23 below show normalised Δ_c and $\dot{\Delta}_c$, for both tests, as calculated from Δ_T in the FEA. The results in these figures show that appreciable creep deformation occurs in both tests. What is most noticeable about both sets of LLD results is that after steadily rising there is a sudden drop. This happens at the point of crack initiation in both scenarios and is caused by creep stress relaxation in the elastic-plastic-creep simulation which will be later discussed. This drop in LLD leads to a negative or near negative creep rate for part of the test.

Comparing Figure 20 and Figure 22, illustrating Δ_c from each test, it can be seen that the longer test exhibited more creep deformation despite the lower stress level due to its significantly longer duration. Post initiation the creep rate continually increases in both tests as the crack growth will lead to increased stresses and therefore accelerated creep deformation.

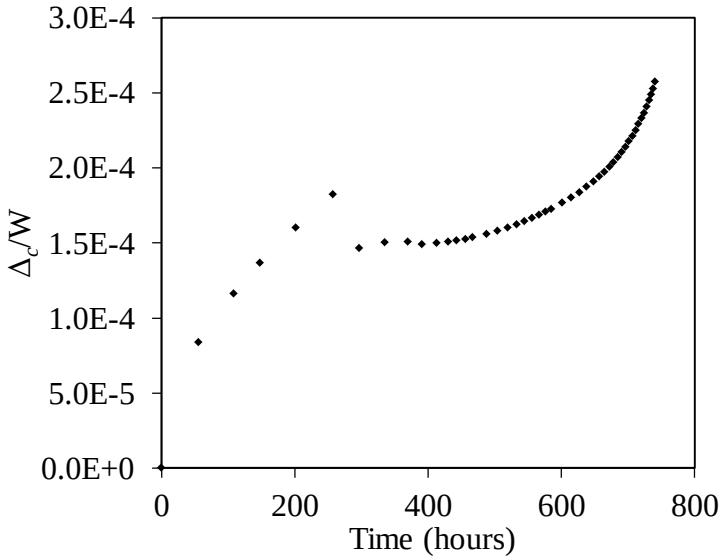


Figure 20 – Short term test FEA normalised creep contribution to the LLD

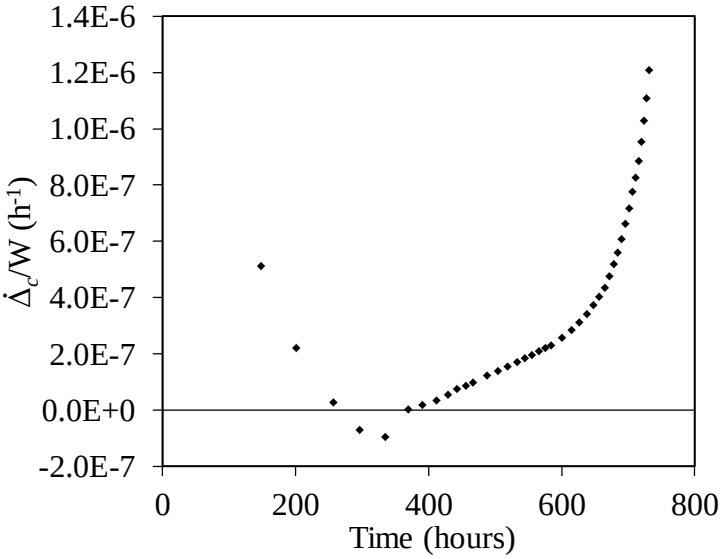


Figure 21 – Short term test FEA normalised creep contribution to the LLD rate

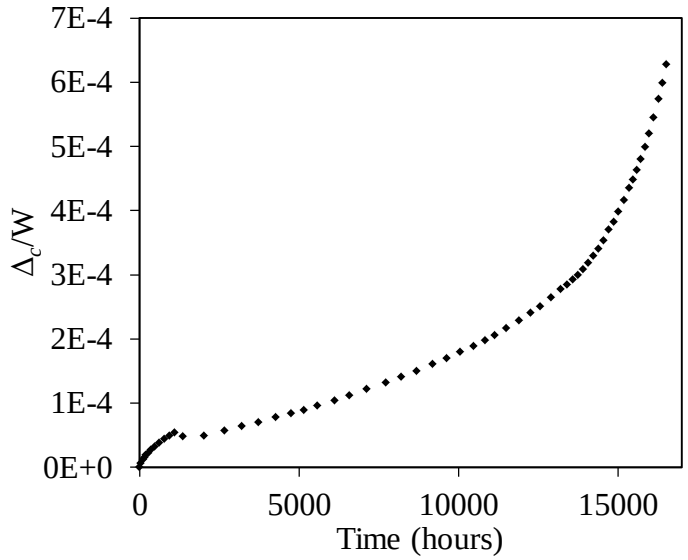


Figure 22 – Long term test FEA normalised creep contribution to the LLD

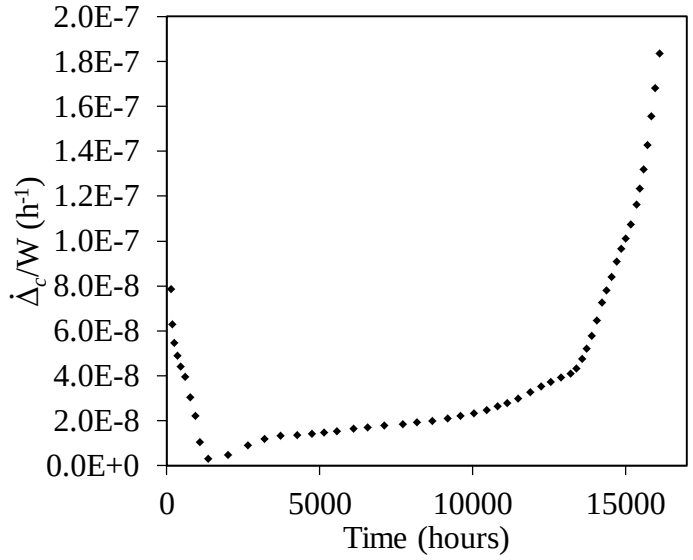


Figure 23 – Long term test FEA normalised creep contribution to the LLD rate

4.3.2. Experimental Contribution

Figure 24 to Figure 27 below show normalised values of Δ_c and $\dot{\Delta}_c$ as calculated by subtracting the FEA determined Δ_{ep} from the total experimental LLD. It is immediately obvious that the creep contribution behaves differently when it is determined from the experimental results. This is due to the disagreement in Δ_T between the FEA and the experimental data, the reasons for which will be discussed in the next section, and that the elastic-plastic FEA contribution exceeds the experimental data in the latter stages of the test, as shown by Figure 28. As such, when it is subtracted from the experimental Δ_T it gives negative results. This leads to $\dot{\Delta}_c$ rates which are either close to zero or negative for the majority of the test.

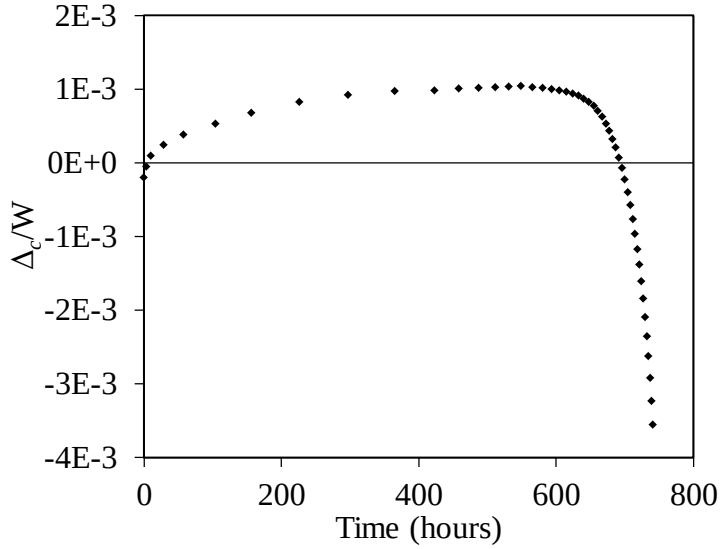


Figure 24 – Short term test experimental normalised creep contribution to the LLD

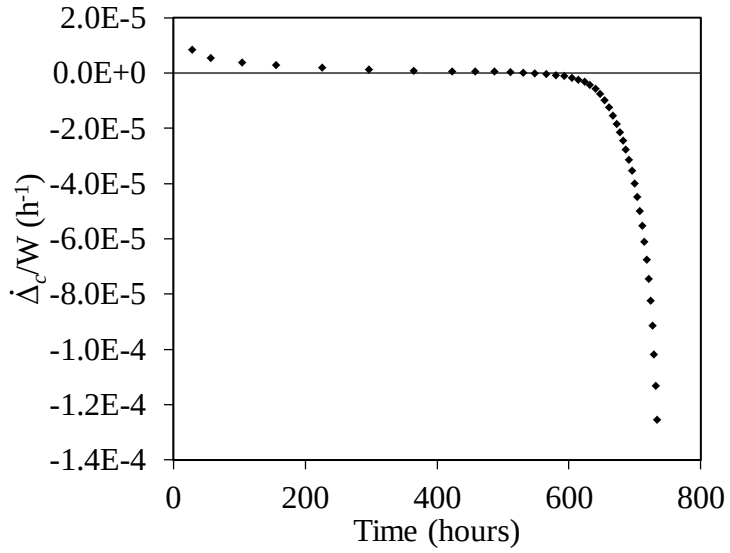


Figure 25 – Short term test experimental normalised creep contribution to the LLD rate

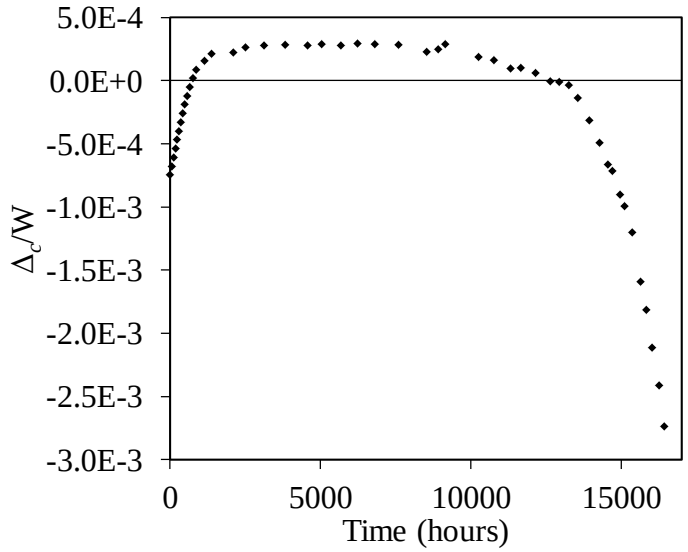


Figure 26 – Long term test experimental creep LLD

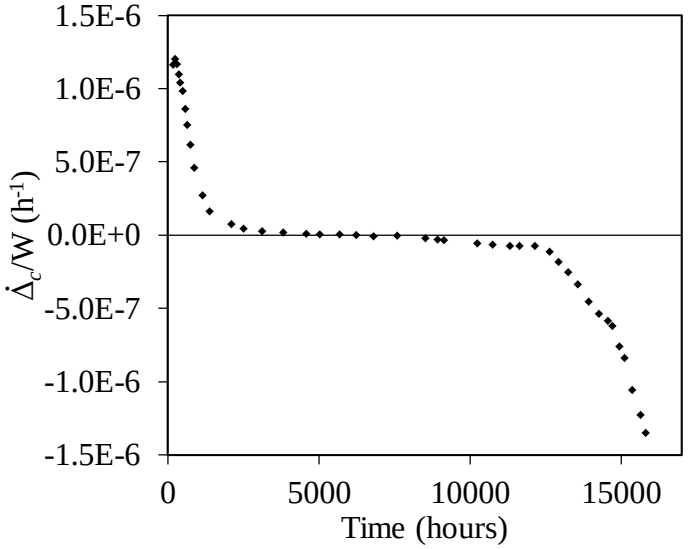


Figure 27 – Long term test experimental creep LLD rate

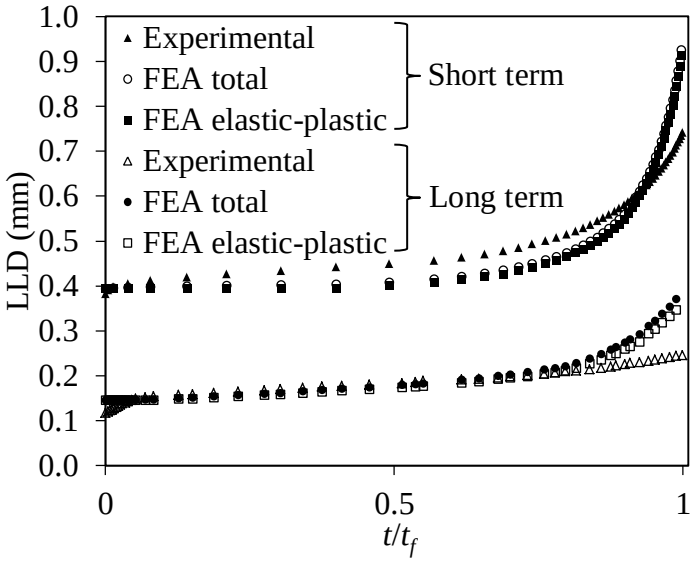


Figure 28 – Comparison of experimental and FEA LLD for long and short term test

5. Discussion

5.1. Elastic Contribution

The results given in Section 4.1.1 show a very small disparity in the Δ_e between the FEA and the EPRI solutions, though theoretically they should be identical. As the solutions are derived for the increase in the distance between the pinholes, the FEA results taken from the crack mouth will inevitably differ slightly. Values taken from the load point in the FEA do produce a better agreement, but ultimately the comparison with experimental data is of more value and as such it is deemed valid to measure values from the crack mouth in line with the experimental technique.

5.2. Plastic Contribution

The results given in Section 4.1.2 highlight the extent to which use of the EPRI solutions, based on a power-law material model fit, overestimates the actual response of the specimen. Not only do the EPRI solutions for the plastic response overestimate the plastic response of the FEA, they overestimate the experimental Δ_T. The reasons for this are the poor fit of a power-law model to experimental uniaxial tensile data, as stated previously, and that the EPRI solutions do not take strain history effects into account.

When a cracked sample is loaded, a plastic zone develops from the crack tip. As crack growth occurs, the new crack tip is growing into the plastic zone leading to a wake of plastic strain which follows the crack tip. Using the EPRI solutions effectively treats each crack tip position during crack growth like a newly loaded sample at said given crack length. This assumes that the crack is growing into previously undeformed material, and therefore no prior strain hardening exists. The prior strain hardening in the FEA prevents the specimen from deforming as much as it would do on load up of a previously unloaded sample at the equivalent length, as illustrated in Figure 29 and Figure 30. Both figures show a contour map of the plastic strain accumulation after an equal number of elements have debonded, and are shown at the same deformation scale factor. The model shown in Figure 29, which uses uniaxial tensile data to model plasticity, exhibits the wake of plastic strain as opposed to the deformation plasticity model in Figure 30, which does not exhibit the wake and has deformed to a much greater extent.

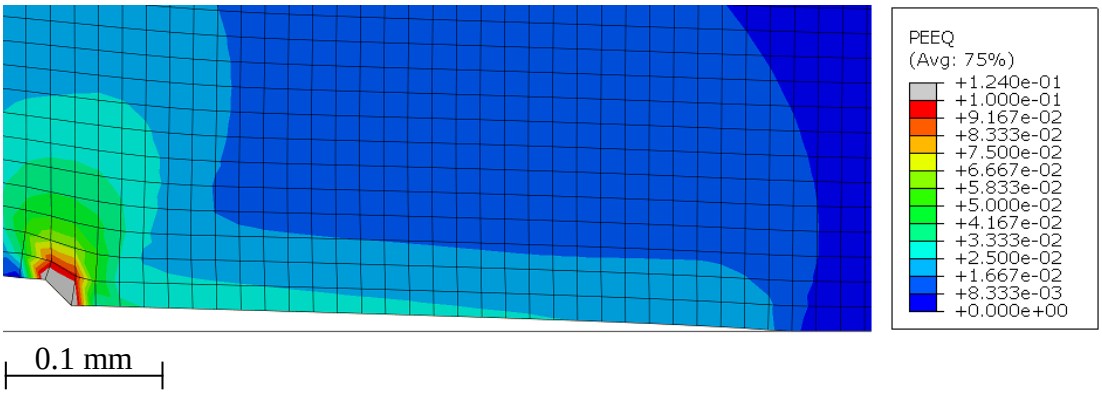


Figure 29 – Plastic strain accumulation in a uniaxial tensile data plasticity FEA model

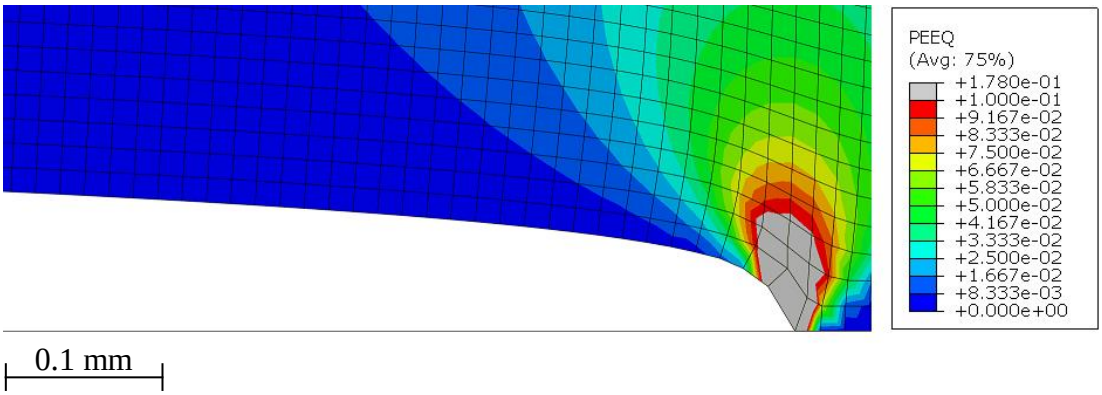


Figure 30 – Plastic strain accumulation in a deformation plasticity FEA model

This shows that use of an incremental plasticity model implemented through FEA and experimental uniaxial tensile data can significantly increase the accuracy of the plastic response of a specimen in a CCG test and reduce the likelihood of obtaining negative values of $\dot{\Delta}_c$.

5.3. Creep Contribution

5.3.1. FEA Contribution

It was shown in Section 4.3.1 that when determining Δ_c from the FEA result for Δ_T, the creep contribution decreased immediately after crack initiation. It has been determined that this is a result of stress relaxation in the creep model, predominantly during the incubation period. The creep deformation and local stress relaxation means that the stresses in the elements near to the crack tip are lower than they are in the elastic-plastic simulation. Consequently, when the y-symmetry boundary condition is removed to grow the crack and a node is released, the crack tip element deforms less than it would do without the creep stress relaxation. Therefore, the assumption that Δ_{ep} is independent of the creep deformation is inaccurate and will lead to an erroneously high value being subtracted.

The solution to this issue is to determine Δ_{ep} from an integrated elastic-plastic-creep analysis. The crack growth formulation works by implementing alternating instantaneous elastic-plastic crack growth steps and time dependent creep steps. For each instantaneous elastic-plastic crack growth step there will be an increase in the LLD as the nodes are progressively debonded, growing the crack. This increase in LLD in the crack growth step is equal to the increase in Δ_{ep} as creep deformation does not occur. The LLD will also increase throughout the duration of the creep steps and, as the crack is not growing, this deformation will be purely due to creep. Therefore the increase in LLD in the creep steps is contributes to Δ_c. The elastic-plastic crack growth steps in the integrated analysis account for the effects of creep stress relaxation, meaning that the overestimate in Δ_{ep} that would be obtained using the results of a separate elastic-plastic analysis is avoided.

Comparisons of the results determined for the elastic-plastic and creep contributions using Δ_{ep} from independent elastic-plastic analyses without any creep behaviour (as described in Table 3), denoted Method 1, and Δ_{ep} from the elastic-plastic steps in the integrated elastic-plastic-creep analyses, denoted Method 2, are shown compared in Figure 31 to Figure 34. It may be seen that the creep contributions are identical in both methods up to initiation as after load-up the specimen only deforms due to creep if the crack is stationary.

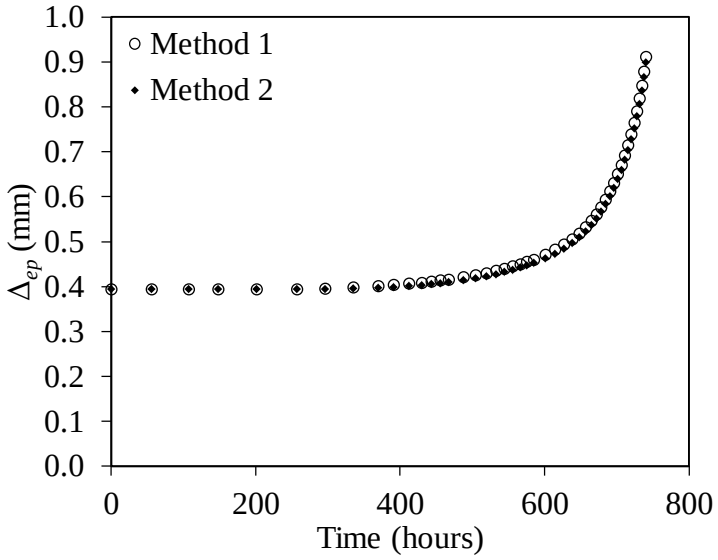


Figure 31 – Short term comparison of the elastic-plastic contribution determined using the old and new method for displacement partitioning

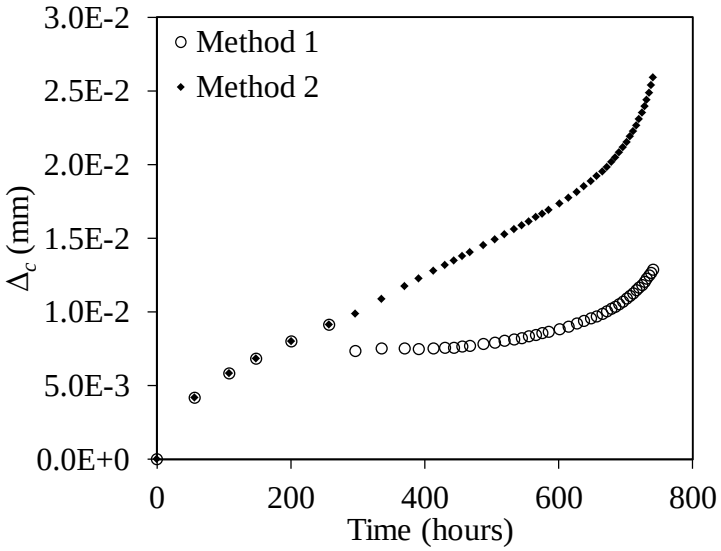


Figure 32 – Short term comparison of the creep contribution determined using the old and new method for displacement partitioning

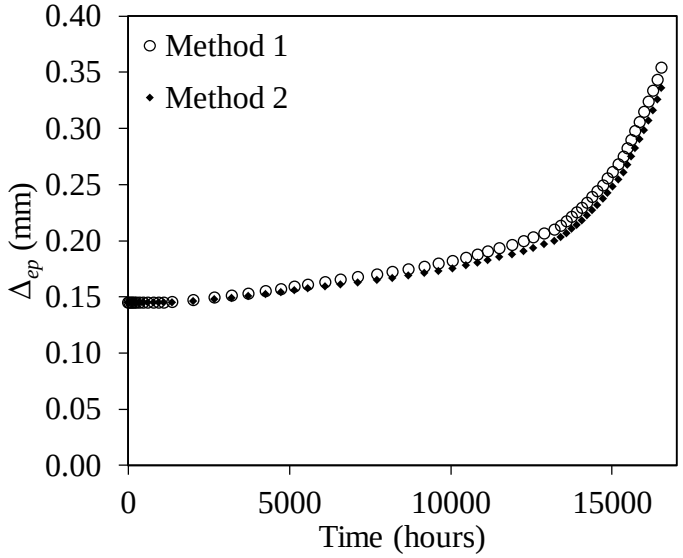


Figure 33 – Long term comparison of the elastic-plastic contribution determined using the old and new method for displacement partitioning

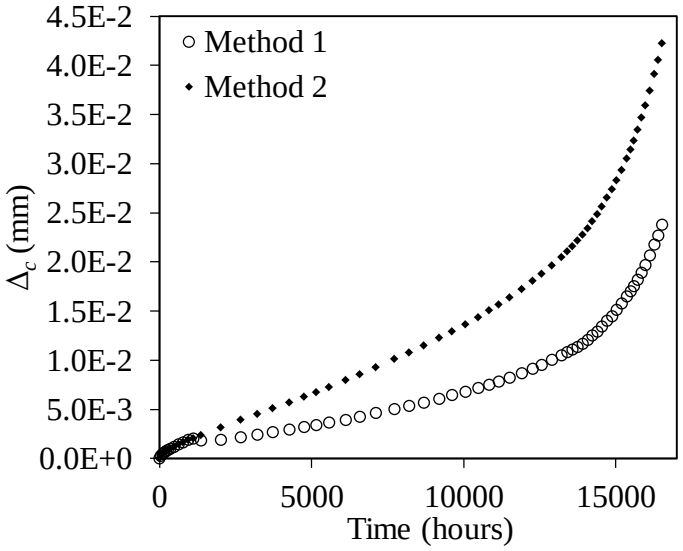


Figure 34 – Long term comparison of the creep contribution determined using the old and new method for displacement partitioning

The above figures show that Method 2 gives reduced values for the elastic-plastic contribution and that the creep contribution no longer exhibits a dip, meaning that the creep rate will remain positive throughout the test.

It should be noted that in the cases considered here the LLD is not dominated by creep effects. The increase of each contribution post load up, normalised with respect to the increase in Δ_T, is shown in Figure 35 and Figure 36 for the short and long term test respectively.

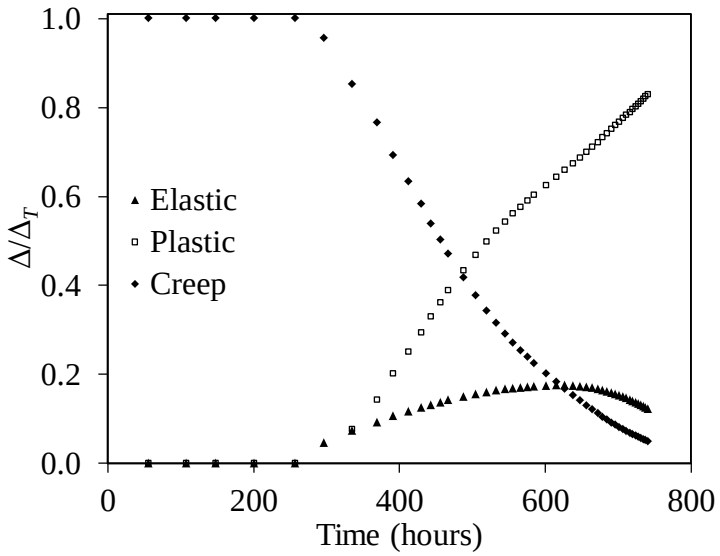


Figure 35 – LLD contributions as a proportion of Δ_T for short term test

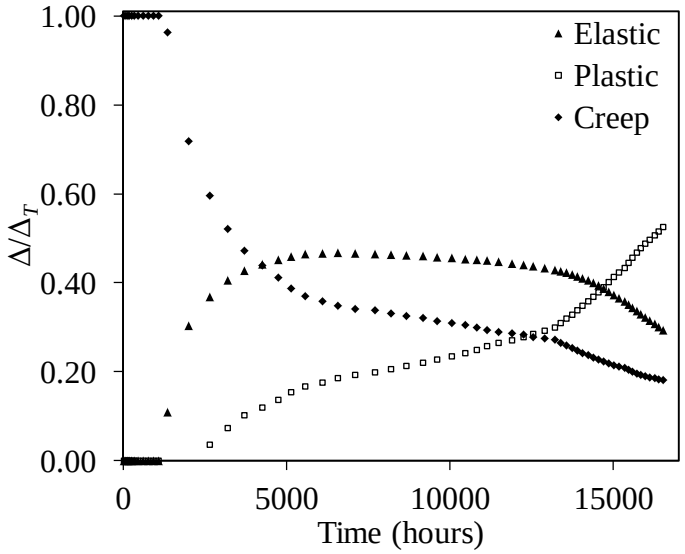


Figure 36 – LLD contributions as a proportion of Δ_T for long term test

For both tests the increase in the LLD is entirely due to creep up until initiation occurs, after which the creep contribution decreases sharply and then continues to fall until the end of the test. For the short term test the normalised Δ_p continually increases up to a final value of 80% of Δ_T, while the normalised Δ_e remains at around 15-20% and the normalised Δ_c decreases to a minimum value of approximately 5%. For the long term test the normalised Δ_p also continually increases but only dominates late on in the test finishing just above 50%, while Δ_e accounts for the majority of the deformation throughout remaining at a level close to 45% of Δ_T with the final normalised Δ_c at around 20%. This may suggest that once a crack initiates, further growth becomes progressively less due to creep and more due to elasticity or plasticity, with a shorter test being more plastic than a longer one due to load being a higher proportion of the limit load. Alternatively, it may suggest that

even though the crack growth may be caused by creep processes the LLD response may be dominated by elastic-plastic deformation.

5.3.2. Experimental Contribution

The main focus of this work is to calculate Δ_{ep} from FEA models and subtract it from experimental Δ_T data to determine Δ_c and thus $\dot{\Delta}_c$ in a CCG test. The new method (Method 2) proposed for displacement partitioning presented in the previous section will improve the accuracy of the experimental creep contribution.

However, challenges exist in simulating the actual LLD response of the experimental tests due to a number of factors including variability in the material's elastic-plastic-creep deformation and hardening behaviour. Though the plastic and creep deformation data employed in the FEA model was obtained from material representative of that of the CCG tests, the elastic-plastic contributions predicted in the FEA exceeded the experimental data for a significant proportion of the test, as shown by Figure 28. Though the new method proposed would improve the Δ_{ep} estimate, the contribution would still exceed the experimental data. The value of $\dot{\Delta}_c$ determined is also negative or close to zero for a large proportion of the test, as once the crack initiates in the FEA simulation the predicted LLD increases faster than the experimental LLD. As a result of the negative $\dot{\Delta}_c$ values, there is little purpose in calculating $\boldsymbol{C}^*$ throughout the test as it will not yield a correlation with the crack growth rate. For the latter parts of the test, the negative values could be a result of the crack morphology, which may be discontinuous and non-planar in the sample. Due to the intergranular nature of the creep damage mechanism, creep cracks are not fully continuous e.g. [3], meaning that ligaments remain behind the crack tip that prevent the LLD from increasing as much as it would do for a continuous crack. The discontinuous cracking process could however lead to additional crack growth and increased PD with much smaller increases in LLD than for a continuous crack.

6. Conclusions

CCG test data analysis requires the accurate determination of the creep contribution to the LLD, Δ_c and LLD rate, $\dot{\Delta}_c$, to determine the creep crack growth characterising parameter, $\boldsymbol{C}^*$. This is achieved by deducting the plastic, Δ_p, and elastic contribution, Δ_e, from the total LLD. The current method for displacement rate partitioning relies on the use of EPRI solutions to determine the plastic contribution, Δ_p. This significantly overestimates the plastic response as the EPRI solutions are based on a Ramberg-Osgood fit which may not accurately represent the material's stress-strain behaviour over a large stress range. Furthermore the EPRI solutions do not take strain history effects into account. Creep cracks grow into strain hardened material leaving an accumulation of

plastic strain behind the crack tip after crack growth. This strain hardening prevents a sample from deforming as much as it would do if it were initially loaded at a given crack length. This is neglected by the EPRI solutions, leading to erroneously high values for Δ_p. It has been demonstrated that even if the Ramberg-Osgood model provided a more accurate fit to uniaxial tensile data, the historical method will still not be able to take the strain history effects into account and as such will give inaccurate results.

A new approach has been proposed that addresses these issues. This new approach implements an incremental plasticity formulation through an FEA model, enabling specific uniaxial tensile test data to be employed. This provides a more accurate material stress-strain response and allows strain history effects to be included, which in turn eliminates the overestimates in Δ_p, and reduces the likelihood of obtaining negative values for $\dot{\Delta}_c$.

It has also been demonstrated that the current standard method of displacement rate partitioning, which assumes that the different contributions to the LLD are independent of each other, is invalid. When Δ_{ep} from an elastic-plastic simulation was subtracted from Δ_T in an elastic-plastic-creep simulation it caused an apparent drop in Δ_c just after crack initiation. This is because stress relaxation occurs around the crack tip in an elastic-plastic-creep simulation, meaning that less plastic deformation will occur when the crack grows as the stresses are lower than they would be without creep deformation. It is not possible to take creep stress relaxation into account when using Δ_{ep} from an elastic-plastic simulation which leads to erroneously high values of Δ_{ep}. The FEA crack growth formulation used for this work performs alternate time dependent creep and instantaneous elastic-plastic crack growth steps. The Δ_c and Δ_{ep} values can be taken incrementally from each of these steps, respectively.

Ultimately the aim is to determine accurate $\dot{\Delta}_c$ values and thus $\boldsymbol{C}^*$ values from experimental tests. This requires strong agreement between the Δ_T values obtained from FEA and experiment. For the test data considered here, some discrepancies existed between the experimental data and FEA predictions. Possible reasons for this are that materials such as 316H exhibit discontinuous cracking, particularly in long term tests, leading to lower LLD values compared to a continuous crack, though the PD response would increase indicating crack growth. Variability may also exist in the material's plasticity and creep deformation behaviour, causing some inaccuracy. Improvements in these areas are expected to further improve the agreement between experimental and numerical results, which will enable CCG relations with $\boldsymbol{C}^*$ determined from short term (high load) laboratory tests to accurately assess CCG under plant operating conditions.

Acknowledgements

The authors thank EDF Energy and EPSRC for providing the funding to conduct the research for this publication. This paper is published with permission from EDF Energy.

7. References

[1] **Nikbin K. M., Smith D. J. & Webster G. A.**, *Prediction of Creep Crack Growth From Uniaxial Creep Data*, Proceedings of the Royal Society A, 1984, Vol. 396, pp. 183-197.

[2] **ASTM**, *E1457-15: Standard Test Method for Measurement of Creep Crack Growth Rates in Metals*, Annual Book of ASTM Standards, 2017, Vol. 3.

[3] **Dean D. W. & Gladwin D. N.**, *Creep Crack Growth Behaviour of Type 316H steels and proposed modifications to standard testing and analysis methods*, International Journal of Pressure Vessels and Piping, 2007, Vol. 84, pp. 378-395.

[4] **Davies C. M., Kourmpetis M., O'Dowd N. P. & Nikbin K. M.**, *Experimental Evaluation of the J or C* Parameter for a Range of Cracked Geometries*, Journal of ASTM International, 2006, Vol. 3.

[5] **Huh N-S., Kim Y-J. & Yoon K-B.**, *Influence of Ramberg-Osgood Fitting on the Determination of Plastic Displacement Rates in Creep Crack Growth Testing*, Fatigue and Fracture of Engineering Materials and Structures, 2007, Vol. 30, pp. 277-286.

[6] **RCC-MR**, *Design and Construction Rules for Mechanical Components of FBR Nuclear Island*, AFCEN, Paris, Section I – Subsection Z: Technical Appendix A3, 1985.

[7] **Norton F. H.**, *The Creep of Steel at High Temperatures*, McGraw-Hill, 1929.

[8] **Kumar V., German M. D. and Shih C. F.**, *An Engineering Approach for Elastic-Plastic Fracture Analysis*, EPRI, 1981, EPRI Report NP-1931.

[9] **Tarnowski K. M., Nikbin K. M., Dean D. W. & Davies C. M.**, *Improvements in the Measurement of Creep Crack Initiation and Growth Using Potential Drop*, International Journal of Solids and Structures, 2017, Vol. 134, pp. 229-248.

[10] **Ritchie R. O., Garrett G. G. & Knott J. F.**, *Crack-Growth Monitoring: Optimisation of the Electrical Potential Technique Using an Analogue Method*, International Journal of Fracture Mechanics, 1971, Vol. 7, pp. 462-467.

[11] **Lowes J. M. & Fearnehough G. D.**, *The Detection of Slow Crack Growth in Crack Opening Displacement Specimens Using an Electrical Potential Method*, Engineering Fracture Mechanics, 1971, Vol. 3, pp. 103-108.

[12] **Austin T. S. P. & Webster G. A.**, *Prediction of Creep Crack Growth Incubation Periods*, Fatigue & Fracture of Engineering Materials and Structures, 1992, Vol. 15, pp. 1081-1090.

[13] **Bettinson A. D.**, *The Influence of Constraint on the Creep Crack Growth of 316H Stainless Steel*, Ph.D. Thesis, Department of Mechanical Engineering, Imperial College London, 2002.